Critical Phenomena in a Spherically Symmetric Gravitational Collapse of Massless Scalar Field

Contents

1 Notes and Disclaimer **4**

2 Introduction **5**

2.1 Notations . . . 5

2.2 Literature Short Overview . . . 5

2.3 Problem and Methods Short Overview . . . 5

3 Theoretical Background **6**

3.1 Cauchy Problem in GR . . . 6

3.2 ADM Formalism . . . 7

3.2.1 Introduction to ADM . . . 7

3.2.2 $3+1$ Decomposition . . . 7

3.2.3 Geometry . . . 9

3.2.4 Einstein Equations in ADM formalism . . . 10

3.3 Slicing . . . 11

3.4 The Spherical Symmetry . . . 12

3.5 Black Hole Horizons . . . 13

3.5.1 Event Horizons . . . 13

3.5.2 Apparent Horizons . . . 13

3.5.3 Apparent Horizon Mathematics . . . 14

3.6 The Double Null (Eddington–Finkelstein) Coordinates . . . 16

3.7 The Mass Function . . . 18

4 Gravitational Collapse Process **19**

4.1 Critical Phenomena in Gravitational Collapse . . . 19

4.1.1 Introduction . . . 19

4.1.2 Types of Critical Phenomena . . . 21

4.2 Massless Scalar Field . . . 22

4.3 Equations Setup . . . 23

5 Numerical Methods **23**

5.1 Preparing Einstein Equations . . . 24

5.2 Boundary Conditions . . . 26

5.3 Initial Conditions . . . 27

5.4 Finite Difference Method . . . 28

5.5 Runge-Kutta methods . . . 29

5.6 Explicit PECECE Method and Stiffness . . . 29

5.7 The Algorithm 31

6 Simulation Results **32**

6.1 Some Technical Notes 32

6.2 Comparing Sub- and Super-Critical Cases 33

6.3 The Critical Behavior 36

6.4 Accuracy of The Calculations 38

7 Appendixes **39**

7.1 Deriving 8^{th} Order Accuracy Centric Finite Difference Approximation 39

1 Notes and Disclaimer

This is a part of another 2015 research work, extracted for the purpose of publishing on GitHub. Only the part related to critical phenomena simulation is listed here.
For the license, simulation raw results, and the source code, which is of two parts, C++ and Wolfram Mathematica, can be found in the following repository:

https://github.com/TMS-Namespace/Critical-Phenomena-in-Gravitational-Collapse

2 Introduction

Critical phenomena is an interesting phenomena that was discovered relatively recently solely through numeric analysis, it lead then to numerous investigations in this field to check if it is a universal phenomena, in a scene if it arises in other gravitational situations. This discovery gained such importance because it was unexpected, and renewed the debates about the possibility of naked singularities' existence.
In this work, we will try to confirm the same results that were previously obtained by similar works.

2.1 Notations

Following the usual conventions, we use the Greek index $\{\mu, \nu \dots\}$ for space-time metrics, and Latin $\{a, b \dots\}$ for space-like metrics, the used metric signature is $(- + ++)$.
In spherical symmetry, we use ρ for radial coordinate (it can take any value), and r for areal coordinate (it can take only zero or positive value).
Note that due to the big number of variables, they can be reused in different paragraphs with different definitions.

2.2 Literature Short Overview

The main idea of the used numerical mythology called *third order explicit predictor-corrector method* (or PECECE) is suggested in [3], and also partly in [15]. Defining the boundary condition and construction of the Cauchy problem can be found in [16].
Equations setup and their classifications to evolution and constraints can be found partially in [2] and [3], also, the obtained results can be compared with the last two references.

2.3 Problem and Methods Short Overview

We use ADM formalism for dimensional reduction of the problem into spatial variables that evolve in time. Furthermore, polar slicing is used for fixing the gauge of time-like coordinates in such a way that there will be no coordinate singularities that may break down the numerical methods.
We will use sign change detection of the expansion to signal apparent horizon and hence black hole formation.
We reduced Einstein's equations with a massless scalar field as a source, into a system of first-order differential equations, and classified them into evolution and constraint equations according to ADM formalism. Then we use Rung-Kuta with explicit PECECE methods to integrate those equations along with a local flatness boundary condition. In addition to that,

we use the finite difference methods to set up these boundary conditions, along with suitable error control.

3 Theoretical Background

Here we introduce briefly some theoretical information related to this work.

3.1 Cauchy Problem in GR

Einstein's equations are a system of nonlinear differential equations. As for any similar equations, to solve them one needs to supply initial conditions. For Cauchy problem setup, we need to specify the metric for a $3-$dimensional hyper-surface at some initial instant t_0 of time: $g_{\mu\nu}\left(t_0\right), \partial_t g_{\mu\nu}\left(t_0\right)$. Then by integrating them forward in time we can obtain $\partial_t^2 g_{\mu\nu}$ at any point. Furthermore, by using Einstein equations we can compute $g_{\mu\nu}\left(t_0+dt\right), \partial_t g_{\mu\nu}\left(t_0+dt\right)$, i.e. at the next moment, and repeat that over and over.
However, calculating $\partial_t^2 g_{\mu\nu}$ is not a trivial task:

- At first glance, one counts 10 differential equations in the Einstein equation $G_{\mu\nu}=8\pi\mathcal{T}_{\mu\nu}$ (symmetric 4×4 tensor), but by recalling the Bianchi identities $G^{\mu\nu}_{;\nu}\doteq 0$ (where $\doteq$ means equals identically), that gives:

$$\partial_t G^{\mu 0}=-\partial_\rho G^{\mu\rho}-G^{\rho\lambda}\Gamma^{\mu}_{\rho\lambda}-G^{\mu\rho}\Gamma^{\lambda}_{\rho\lambda}$$

  we notice that the right-hand side contains at most second-order time derivatives, and hence, each of the four quantities of $G^{\mu 0}$ can contain at most first-order time derivatives. This means that the 4 equations $G^{\mu 0}=8\pi\mathcal{T}^{\mu 0}$ contains no information about the dynamical evolution of the fields, and thus they actually provide constraints on the initial conditions, that is, initial conditions can't be chosen freely

- On another hand, this means that we have actually only 6 equations that describes the evolution $G^{ab}=8\pi\mathcal{T}^{ab}$, this ambiguity for the other 4 equations actually raises due to the freedom of choosing the 4 coordinates.

- However, among the $6+6=12$ functions of $g_{ab}, \partial_t g_{ab}$, there are actually only 2 true dynamical degrees of freedom that can be initially specified on the hyper-surface: we can specify 3 arbitrary spatial coordinate transformations within the hyper-surface, without affecting its geometry, additionally, there is a freedom in our choice of how to embed the initial hyper-surface in space-time (the isometric/conformal invariance). Thus we are left with $12-4-3-1=4$ dynamic degrees of freedom (two sets of two functions

for $g_{ab}, \partial_t g_{ab}$). The two true degrees of freedom do characterize the gravitational field, and corresponds to the two polarization states of gravitational waves.

3.2 ADM Formalism

A crucial role in current numerical analysis plays space-time decomposition, because it allows us to rewrite Einstein's equations in a more intuitive way: when spatial variables evolve in time.

3.2.1 Introduction to ADM

Arnowitt, Deser, and Misner introduced a $3+1$ (space plus time) slicing or decomposition of space-time metric, it provides a natural way of splitting, which is induced by the Einstein equations (as pointed out in the previous paragraph) by focusing on the 12 purely spatial quantities. This formalism raised from the analysis of the Cauchy problem, same as we did above, along with the efforts toward constructing a Hamiltonian formulation of general relativity, to build quantum gravity. Also, a similar setup can be built in Maxwell equations. Below we provide a brief introduction to it.

3.2.2 $3+1$ Decomposition

If we slice/foliate space-time, that equipped with the coordinates (x^a, t) into a family of space-like hypersurfaces as $T \times \Sigma$, then we can define a time like, closed one-form $\nabla_\alpha t$, and then we can also define a unit norm vector, based on it. This norm will be dual to the covariant normal vector field:

$$n_\mu \equiv -\alpha\,(x) \cdot \nabla_\mu t$$

where α is a normalization factor such that $n^\mu n_\mu \equiv -1$, and $x \equiv \{x^\mu\}$. Additionally, we assume that $\alpha > 0$ so $\nabla_\mu t$ will be time-like everywhere.
Since n is a unit time-like vector, we can think about it as a $4-$velocity of some observer, those observers called *Eulerian observer* (or *fiducial*, or *locally non-rotating*, or *zero-angular-momentum* observer). This makes world-lines of Eulerian observers to be orthogonal to the hyper-surfaces, and physically this means that locally speaking, Σ is a set of events that are simultaneous from the Eulerian observer's point of view [8].

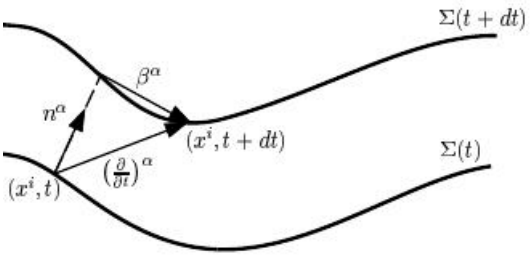

Figure 1: A slice of the hyper-surface $\Sigma(t)$, and the vector $(\partial/\partial t)^\mu = \alpha(x)\, n^\mu + \beta^\mu(x)$ that describes how the time flows at some point (x^a, t), in a constant spatial direction, within the whole family of hyper-surfaces.

Any vector field that transects (lies nowhere in) the foliation, can be decomposed into orthogonal and parallel components (see figure 1), and by considering the time-like Lie derivative vector field, that will be tangent to the constant spatial lines, we can put ($\equiv$ symbols a definition):

$$\left(\frac{\partial}{\partial t}\right)^\mu \equiv \alpha(x)\, n^\mu + \beta^\mu(x) \tag{1}$$

where:

- $\alpha(x)$ is called the *lapse function*, describes the lapse of proper time, per unit coordinate time, relative to an observer that moves normally to the slices. It's easy to see that the lapse function can absorb the freedom of time coordinate rescaling.
- $\beta^\mu(x)$ is the *shift vector*, describes the shifting of spatial coordinate, relative to the normal propagation. In other words, it determines how relative to some normal observer n, the spatial points are relabeled on neighboring slices. Also, we can see that it embodies the 3 coordinate degrees of freedom within the space-like hyper-surface. Also, note that it's actually a spatial vector ($\beta^\mu n_\mu = 0$).

To decompose tensors into tangential (spatial) and the orthogonal/temporal parts, we define a *projection tensor*, it will project any space-time manifold with metric $g_{\mu\nu}$, onto a tangent tensor (called *spatial tensor*) on the space-like hyper-surface, with an *induced/intrinsic* metric h_{ab} :

$$\Pi_{\mu\nu} \equiv g_{\mu\nu} + n_\mu n_\nu$$

(note that the $+$ sign is due to the metric signature $(-+++)$) and the "projection" behavior is clear from the fact that $\Pi_{\mu\nu} n^\mu = \Pi_{\mu\nu} n^\nu = 0$.
Thus, for an arbitrary tensor $T_{\alpha\beta\ldots}^{\ \ \ \gamma\delta\ldots}$, the spatial part is seen as:

$$\perp T_{ab\ldots}^{\ \ \ cd\ldots} \equiv \Pi^\alpha_{\ a} \Pi^\beta_{\ b} \ldots \Pi_\gamma^{\ c} \Pi_\delta^{\ d} \ldots T_{\alpha\beta\ldots}^{\ \ \ \gamma\delta\ldots}$$

and the contraction of any of its indexes with n^α, will vanish.

Finally, the induces spatial metric, is just a projection of the original (*extrinsic metric*) one:

$$h_{ab} = \Pi^{\mu}_{\ a}\Pi^{\nu}_{\ b}\, g_{\mu\nu}\ ,\ h_{ac}h^{cb} = \delta^{b}_{a}$$

3.2.3 Geometry

To specify the resultant geometry, one can define the $3-$derivative as a projection of the usual covariant derivative:

$$D_{\mu} \equiv g^{\nu}_{\mu}\nabla_{\nu}$$

This allows us to define a spatial Riemann tensor, by its action on an arbitrary dual-vector ω_a, by using the commutators:

$$^{(3)}\mathcal{R}_{\mu\nu\rho}^{\ \ \ \lambda}\,\omega_{\lambda} \equiv [D_{\mu}, D_{\nu}]\,\omega_{\rho}$$

where the "(3)" symbol that located on the right hand side of tensors, points to the tensors' dimentionality.
Also, the spatial Ricci tensor and scalar, becomes: $^{(3)}\mathcal{R}_{\mu\nu} \equiv {}^{(3)}\mathcal{R}_{\mu\lambda\nu}^{\ \ \ \lambda}$, $^{(3)}\mathcal{R} \equiv {}^{(3)}\mathcal{R}^{\mu}_{\mu}$.
Next, we define the *Extrinsic curvature*, that describes how the $3-$dimensional hyper-surfaces are embedded in the $4-$dimensional space-time, by describing how the normal gradient varies (varies in directions only, since it's normalized) along the hyper-surface (see figure 2):

$$\mathcal{K}_{\mu\nu} \equiv -D_{\mu}n_{\nu}$$

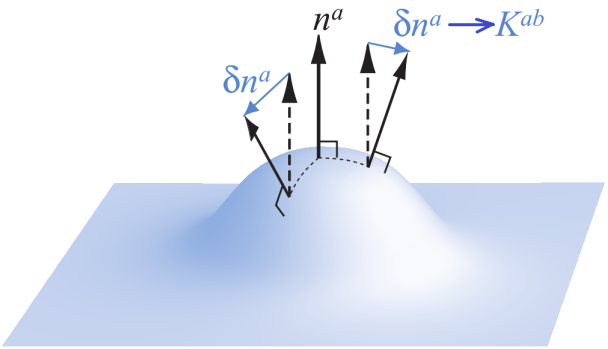

Figure 2: The extrinsic curvature of a hyper-surface, that measures how much a normal vector to the hyper-surface differs at neighboring points [4].

this curvature can be also expressed by Lie derivative of the intrinsic metric:

$$\mathcal{K}_{ab} = -\frac{1}{2}\mathcal{L}_{n}h_{ab} \tag{2}$$

its trace: $\mathcal{K} \equiv \mathcal{K}^{\mu}_{\mu}$ is called *mean curvature*, and can be understood as a fractional change of

the proper $3-$volume along n [4].
By recalling the *Gauss and Codazzi equations* [4], one can conclude that the extrinsic curvature $\mathcal{K}$ and the intrinsic metric h are enough to determine the gravitational field as a dynamical system, and that they are our true dynamical variables. While the lapse and shift functions, are gauge variables, since they are related to the freedom in the coordinate choice [1].

3.2.4 Einstein Equations in ADM formalism

In this formalism, Einstein equations will be split into two groups:

1. Constraint equations: which must be fulfilled at every time slice hyper-surface, and thus they will involve only spatial derivatives. Those constraints by themselves, are of a two types:

   (a) Hamiltonian Constraints: that raises if we contract Einstein equations as follows:

   $$\begin{aligned} n^\mu n^\nu \left(G_{\mu\nu} + \Lambda g_{\mu\nu} - 8\pi \mathcal{T}_{\mu\nu}\right) &= 0 \\ \Rightarrow {}^{(3)}\mathcal{R} + \mathcal{K}^2 - \mathcal{K}^a_b \mathcal{K}^b_a - 2\Lambda &= 16\pi\rho \end{aligned} \tag{3}$$

   where: $\rho \equiv n^\mu n^\nu \mathcal{T}_{\mu\nu}$ is the energy density.

   (b) Momentum constraints: can be obtained also by the following contractions:

   $$\begin{aligned} n^\mu g^\rho_\nu \left(G_{\mu\rho} + \Lambda g_{\mu\rho} - 8\pi \mathcal{T}_{\mu\rho}\right) &= 0 \\ \Rightarrow D_b \mathcal{K}^{ab} - D^a \mathcal{K} &= 8\pi j^a \end{aligned}$$

   where $j^\mu \equiv n^\mu g^\rho_\nu \mathcal{T}_{\mu\rho}$ is the momentum density.

2. Evolution equations: which will evolve the extrinsic curvature and intrinsic metric, from one hyper-surface to another. There is also two of them:

   (a) Intrinsic spatial metric evolution: we note that by considering the following coordinate system (t, x^a), and from (1) and (2), the extrinsic curvature and intrinsic metric can be related by:

   $$\mathcal{L}_t h_{ab} = 2\alpha \mathcal{K}_{ab} + \mathcal{L}_\beta h_{ab} \tag{4}$$

   (b) Extrinsic curvature evolution: which are obtained by the following contractions:

   $$g^\lambda_\mu g^\rho_\nu \left(G_{\lambda\rho} + \Lambda g_{\lambda\rho} - 8\pi \mathcal{T}_{\lambda\rho}\right) = 0$$

this gives:

$$\begin{aligned}\mathcal{L}_t\mathcal{K}^a_b &= \mathcal{L}_\beta\mathcal{K}^a_b - D^aD_b\alpha + \\ &\quad +\alpha\left\{{}^{(3)}\mathcal{R}^a_b + \mathcal{K}\mathcal{K}^a_b - 2\mathcal{K}^a_c\mathcal{K}^c_b + 4\Lambda - 8\pi\left[S^a_b - \frac{h^a_b}{2}(S-\rho)\right]\right\}\end{aligned}$$

where $S^{\mu\nu} \equiv g^\mu_\rho g^\nu_\lambda \mathcal{T}^{\rho\lambda}$ is the stresses along the hyper-surface.

Note that all of the derived equations are first order, and they are equivalent for original Einstein second order equations.

3.3 Slicing

Slicing choice (or choosing/fixing gauge for the time coordinate), is restricted by multiple criteria and points of interest:

- First of all, we need to avoid any possible coordinate singularities, that will break any numerical methods.
- We would like to make the resultant equations simpler, and the calculations less resources consuming.
- Self-symmetry behavior (as will be explained later on), that the the system can exhibit during the gravitational collapse, also should be taken in account [17]

Anyway, achieving such a well-behaved approach even during a long time of evolution. is not a trivial task. So, to address these issues, different slicing methods are developed, such as geodesic, maximal, polar, harmonic, minimal distortion...etc.
For example, to avoid the coordinate singularities that are usually associated with horizons (such as $r_h = 2m$ in the Schwarzschild case), one will need to use *horizon penetrating* (or *regular across*) coordinate system, for which light cones will not pinch-off at the horizon.
In this work, we will adopt the *polar slicing*, which is usually associated with the spherical symmetry (ρ, θ, φ), and defined by:

$$\mathcal{K}^\theta_\theta = \mathcal{K}^\varphi_\varphi = 0 \Rightarrow \mathcal{K} = \mathcal{K}^\rho_\rho \tag{5}$$

This slicing has a couple of advantages, one of which is the avoidance of the trapped surfaces, and hence avoids the singularities during the black hole formation. In addition to that, the metric in this slicing will take an isotropic Schwarzschild form (with $\mathcal{K}^r_r = 0$) everywhere in the exterior vacuum. This means, that we will need to integrate Einstein equations only within the matter, then we match the rest of the space with the standard Schwarzschild metric, when we use the isotropic coordinates.

3.4 The Spherical Symmetry

Using the previous results, we got the following $3+1$ decomposition of the metric:

$$\begin{aligned} ds^2 &= g_{\alpha\beta}dx^\alpha dx^\beta \\ &= -\alpha^2(x)\,dt^2 + h_{ab}\left(dx^a+\beta^a dt\right)\left(dx^b+\beta^b dt\right) \\ &= \left[-\alpha^2(x)+\beta_a\beta^a\right]dt^2 + 2\beta_a\,dx^a dt + h_{ab}\,dx^a dx^b \end{aligned}$$

then evolution of the spatial metric (4) can be then written as:

$$\partial_t h_{\mu\nu} = -2\alpha\mathcal{K}_{\mu\nu} + D_\mu\beta_\nu + D_\nu\beta_\mu \tag{6}$$

So, this decomposed metric can be well simplified in the spherical symmetry, by throwing away the S^2 topology (during the simulation), hence reducing the problem to only $1+1$ dimensions.
Clearly, here the foliations Σ became hyper-lines instead of hyper-surfaces, then, the shift vector will have only one component: $\beta^a \equiv (\beta,0,0)$. By supposing that $h^{00} \equiv a^2(r,t)$, the most general form of ADM decomposition, in the spherical-polar coordinates, can be written as:

$$ds^2 = \left(-\alpha^2+a^2\beta^2\right)dt^2 + 2a^2\beta dt d\rho + a^2 d\rho^2 + r^2(\rho,t)\,d\Omega^2 \tag{7}$$

where $d\Omega^2 \equiv \sin^2\theta d\xi^2 + d\theta^2$ is the unit $2-$sphere element, and r is the *areal coordinate*.
However, in spherical symmetry, space-time can't radiate no matter how violently it may be evolving (due to *Birkhof theorem*), and thus no gravitational waves can be emitted. Consequently, it possesses no dynamical degrees of freedom at all. Hence, among the apparent 6 degree of freedom in the spatial metric (3 gauges from the shift vector, the two dynamical degrees of freedom, and finally the conformal factor), only one of them is the true degree of freedom, which is the conformal factor $a(\rho,t)$. So, we actually don't need to solve the evolution equations of the spatial metric a, or even the equations of the extrinsic curvature $\mathcal{K}^\rho_\rho$, since they can be determined on each time slice, entirely by the previously obtained Hamiltonian and momentum constraints.
Furthermore, by using the last metric expression, from (6) we can find that:

$$\mathcal{K}_{\theta\theta} = \frac{\mathcal{K}_{\varphi\varphi}}{\sin^2\theta} = \beta\frac{\rho}{\alpha a}$$

from which follows immediately, that we should have $\beta = 0$ due to our slicing condition (5), and this converting the metric (7) into a simpler diagonal form:

$$ds^2 = -\alpha^2(\rho,t)\,dt^2 + a^2(\rho,t)\,d\rho^2 + r^2(\rho,t)\,d\Omega^2 \tag{8}$$

3.5 Black Hole Horizons

3.5.1 Event Horizons

Black holes are characterized by their event horizons, and they are defined by a boundary in space-time beyond which events cannot affect an outside observer. Or equivalently, no null geodesic can escape to infinity, thus, it is a boundary $2+1$ hyper-surface that is formed by the outward-going, future-directed, null geodesics, that will not be able to escape to infinity, or even fall into the center of the black hole. It's important to note that it is a gauge-invariant object.

However, due to its global nature, it's difficult to locate the horizon during the numeric simulations. This happens because one needs to track the null geodesics along the whole space-time, to be able to decide whether or not it will escape to infinity, This also means that we need to follow the evolution process, long enough to arrive to some stationary state, and only after that, one can check for event horizon formation. Also, it is worthy to note that in general, event horizon evolution in time, doesn't need to be a continuous process, and it can make desecrate jumps.

Additionally, the knowledge of the event horizon (even approximately), will allow us to cut off the internal region of the black hole (*excision technique*) during simulations. This can be done, due to the fact that what is inside a black hole, is casually independent of what is outside, and thus the outer regions evolve independently. The benefit of that is the ability to avoid singularities that leads to the break down of numerical methods (anyway, in this work, this is not needed, due to the chosen coordinate system as we will see letter on).

3.5.2 Apparent Horizons

To avoid the issue of finding the event horizon, we can search for the apparent horizons instead (there are actually many other types of horizons that can be checked, however, this one is sufficient in this work). This approach is motivated by the *singularity theorem of general relativity* [5], which states that if the apparent horizon exists on some time slice, then it should be inside the black hole's event horizon. However, one should be aware that the opposite is not true: the absence of an apparent horizon doesn't imply the absence of the event horizon (this may happen even in the Schwarzschild geometry with a special slicing, see [16] for a detailed simulation results on this).

Note that the apparent horizon is actually gauge-dependent, and also slice-dependent (as in the above example), however, this is not an issue, since we know that in a stationary

space-time, event and apparent (if exists) horizons coincide, and hence apparent horizon will eventually appear on some slice during the evolution.

3.5.3 Apparent Horizon Mathematics

Consider a closed and smooth $2-$dimensional spatial hyper-surface S, that embedded in a hyper-surface Σ. And let s^a be a unit vector normal to S that pointing outward, and lying in Σ (see figure 3). Also let n^a be a unit normal vector to the hyper-surface Σ, hence we have $s^a s_a = 1,\ s^a n_a = 1$.

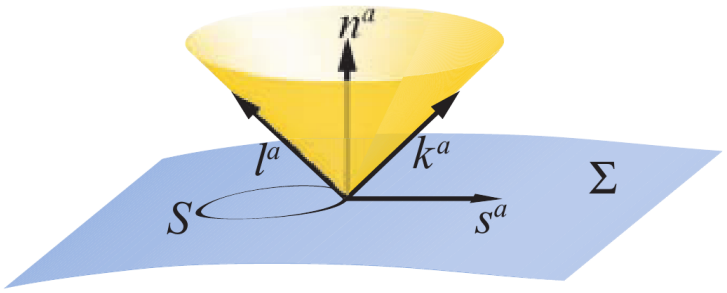

Figure 3: A demonstration of the unit outgoing and ingoing null tangent (to null geodesics) vectors l^μ, k^μ to the surface S that embedded inside the hyper-surface Σ [4].

By using the same scheme we used in $3+1$ decomposition, when $g_{\mu\nu}$ induced the spatial metric h_{ab}, the metric h_{ab} now can also induce a $2-$dimensional metric w_{ab} on S by:

$$w_{\mu\nu} = h_{\mu\nu} - s_\mu s_\nu = g_{\mu\nu} + n_\mu n_\nu - s_\mu s_\nu$$

Now from each point on S, we can define a set of tangent vectors to the light cone, that goes out of Σ. In this set, we can define tangent' outgoing and ingoing vectors to the null geodesics, and they will be future-pointing vectors:

$$k^\mu \equiv \frac{n^\mu + s^\mu}{\sqrt{2}}\ ,\ l^\mu \equiv \frac{n^\mu - s^\mu}{\sqrt{2}}$$

where $k^\mu k_\mu = l_\mu l^\mu = w_{\mu\nu} k^\mu = w_{\mu\nu} l^\mu = 0$ and $k^\mu l_\mu = -1$. It should be noted that those two vectors, will point into the black hole interior if they are inside it (see figure 4).
By using the above, it's easy to rewrite S metric in terms of these vectors:

$$w_{\mu\nu} = g_{\mu\nu} + k_\mu l_\nu + l_\mu k_\nu$$

Now we define the *expansion* of the outgoing null geodesics that are orthogonal to S as:

$$\Theta \equiv w^{\mu\nu}\nabla_\mu k_\nu$$

considering that the sign (but not the value) of the expansion is a geometric invariant [13]. If $\Theta > 0$, the outgoing rays diverge, but the ingoing rays do converge (see figure 4). However, if there is an object of a very strong gravitational field, the outgoing rays may converge too, this happens when $\Theta < 0$ as well. Then, we call S as the *outer-trapped surface* (or *trapped null surface*, where *null surface* means a spatial surface for which every normal vector will be a null vector). Finally, the outgoing rays will be parallel when $\Theta = 0$, and then we have a *marginal or marginally trapped surface* (since outgoing null geodesics vanishes).
So, if we define a *trapped region*, to be any region of Σ that contains the outer trapped surfaces, then we define the *apparent horizon* as the outer boundary (the outermost) of all connected trapped regions.

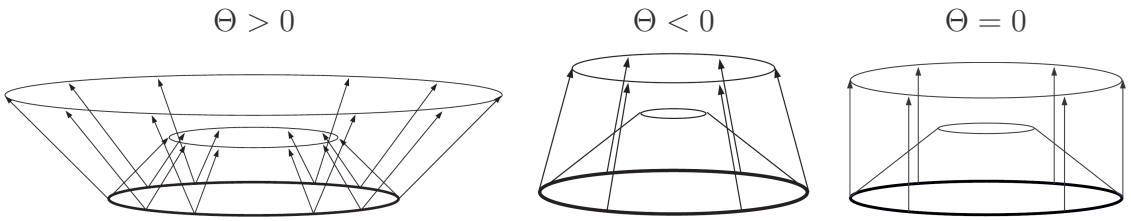

Figure 4: A schematic explanation for the different possible null expansions (observers considered to be inside) [6]

Now we can apply this definition on the metric (7), for that, we consider a sphere that is centered at the origin, then the induced metric is:

$$w_{\mu\nu} = \text{diag}\left(0, 0, r^2, r^2\sin^2\theta\right)$$

and the spatial normal vector can be written as:

$$s^\mu = \left(0, \frac{1}{a}, 0, 0\right) \Rightarrow s_\mu = (a\beta, a, 0, 0)$$

and the outgoing null normal is:

$$k_\mu = \frac{1}{\sqrt{2}}\left(a\beta - \alpha, a, 0, 0\right) \ , \ k^\mu = \frac{1}{\sqrt{2}}\left(\frac{1}{\alpha}, \frac{1}{a} - \frac{\beta}{\alpha}, 0, 0\right)$$

finally, the expansion will be:

$$\Theta = \frac{\sqrt{2}}{r}\left[\frac{1}{\alpha}\frac{\partial r}{\partial t} + \left(\frac{1}{a} - \frac{\beta}{\alpha}\right)\frac{\partial r}{\partial \rho}\right] \tag{9}$$

As an example, if we take Schwarzschild black hole in anisotropic coordinates:

$$ds^2 = -\left(\frac{2\rho - m}{2\rho + m}\right)^2 dt^2 + \left(1 + \frac{m}{2\rho}\right)^4 \left(d\rho^2 + \rho^2 d\Omega^2\right)$$

then we have $a = \gamma = (1 + m/2\rho)^2, \beta = \partial_t r = 0$, and the apparent horizon condition gives $\partial_\rho r = 0 \Rightarrow r_h = m/2$, that is, it coincides with the event horizon, since space-time is static, as we mentioned above.

3.6 The Double Null (Eddington–Finkelstein) Coordinates

Unlike *Bondi coordinates* that cannot penetrate apparent horizons, since its areal radial coordinate misbehaves near the apparent horizon. However, double null coordinates can avoid this.

Double null coordinates, are constructed by using both *outgoing and ingoing* coordinates (or *Bondi coordinates*) as follows:

$$\begin{cases} u \equiv t - \rho^* \\ v \equiv t + \rho^* \end{cases} \Rightarrow \begin{cases} t = (v + u)/2 \\ \rho^* = (v - u)/2 \end{cases} \tag{10}$$

Note that if $\rho = r$ (that is, if it is an areal coordinate), and since by definition $r = (v - u)/2 \geq 0 \Rightarrow v \geq u$. So, by this we can reduce the amount of the needed calculations, since we don't need anymore, to cycle over the whole (u, v) grid, but only half of it is needed now. Furthermore, note that $u = v \Rightarrow r = 0$, this is called to be *on axis*.

For example, the flat line element in spherical coordinates, can be written as:

$$ds^2 = -dudv + r(u, v)^2 d\Omega^2 \tag{11}$$

hence, it's clear that the ingoing/outgoing radial null geodesics will be given by $u/v = const$. To use them with Schwarzschild metric:

$$ds^2 = -\left(1 - \frac{2m}{r}\right) dt^2 + \left(1 - \frac{2m}{r}\right)^{-1} dr^2 + r^2 d\Omega^2 \tag{12}$$

we first redefine the radial coordinate by *Tortoise coordinate* (or *Regge-Wheeler coordinate*) as follows:

$$\frac{dr^*}{dr} \equiv \left(1 - \frac{2m}{r}\right)^{-1} \Rightarrow r^* = r + 2m \ln\left(r - 2m\right)$$

where $r^* \underset{r\to 2m}{\longrightarrow} -\infty$, so we see that it was chosen such that it will grow at an appropriate rate to cancel out the singular behavior in the original coordinate system, and hence it's name. Furthermore, by using r^* instead of r in the double null coordinate definition, gives us:

$$ds^2 = -\left(1 - \frac{2m}{r\left(u,v\right)}\right) dudv + r\left(u,v\right)^2 d\Omega^2$$

hence, in this coordinate system, Schwarzschild metric is actually conformally flat, when we have $\Omega = const$. And also we notice that there is no coordinate singularities to worry about. Generally, the line element (8) can be converted to the following simpler form:

$$ds^2 = -\alpha^2\left(u,v\right)\, dudv + r^2\left(u,v\right) d\Omega^2 \tag{13}$$

and by using the general Tortoise coordinate (that will make non-symmetric part of line element become conformally flat), we get:

$$\frac{d\rho^*}{d\rho} = \frac{a}{\alpha} \tag{14}$$

now, we can apply double null coordinates (10).
The proper time in the metric (13) is defined by:

$$T \equiv \int\limits_{(\ell)} ds = \int\limits_{(\ell)} \alpha\left(u,v\right)\sqrt{du\, dv}$$

where ℓ is some space-time line. If we chose this line to be such that the areal coordinate is $r = const$, and by noticing that the equality $r = r\left(u,v\right)$ can be inverted as $v = v\left(u,r\right)$, then on this line we can also write $dv = \left(\partial v/\partial u\right)_r du$, what allows to rewrite the proper time as:

$$T\left(u\right)\big|_{r=const} = \int\limits_0^u \alpha\left(\omega, v\left(\omega,r\right)\right)\sqrt{\left(\frac{\partial v\left(\omega,r\right)}{\partial\omega}\right)_r}\, d\omega \tag{15}$$

where we considered that the variable u plays the role of the evolution/time variable.
Now we want to analyze how the apparent horizon condition becomes in those coordinates. We have here $\beta = 0$, thus (9) becomes:

$$\Theta = \frac{\sqrt{2}}{r}\left[\frac{1}{\alpha}\frac{\partial r}{\partial t} + \frac{1}{a}\frac{\partial r}{\partial \rho}\right] = 0$$

and by using (10), we can rewrite this equation as:

$$\frac{1}{\alpha}\left(\frac{\partial r}{\partial u}\frac{\partial u}{\partial t} + \frac{\partial r}{\partial v}\frac{\partial v}{\partial t}\right) + \frac{1}{a}\left(\frac{\partial r}{\partial u}\frac{\partial u}{\partial \rho} + \frac{\partial r}{\partial v}\frac{\partial v}{\partial \rho}\right) = \frac{1}{\alpha}\left(\frac{\partial r}{\partial u} + \frac{\partial r}{\partial v}\right) + \frac{1}{a}\left(\frac{\partial r}{\partial u}\frac{\partial u}{\partial \rho} + \frac{\partial r}{\partial v}\frac{\partial v}{\partial \rho}\right) = 0$$

but, noticing that both of $\rho\left(u,v\right), \rho^{*}\left(u,v\right)$, can be inverted to get $u\left(\rho,v\right) = \tilde{u}\left(\rho^{*},v\right)$, and by using (10) and (14) we can write that:

$$du\left(\rho,v\right) = d\tilde{u}\left(\rho^{*},v\right) \Rightarrow \frac{\partial u}{\partial \rho}d\rho = \frac{\partial \tilde{u}}{\partial \rho^{*}}d\rho^{*} = -d\rho^{*} = -\frac{a}{\alpha}d\rho \Rightarrow \frac{\partial u}{\partial \rho} = -\frac{a}{\alpha}$$

similarly, we can find that $\partial v/\partial \rho = a/\alpha$. Substituting this back in the apparent horizon criteria, we get:

$$\frac{1}{\alpha}\left(\frac{\partial r}{\partial u} + \frac{\partial r}{\partial v}\right) + \frac{1}{a}\left(-\frac{a}{\alpha}\frac{\partial r}{\partial u} + \frac{a}{\alpha}\frac{\partial r}{\partial v}\right) = \frac{1}{\alpha}\frac{\partial r}{\partial v} = 0$$

hence, the apparent horizon condition, in the double null coordinates reduces simply to:

$$\frac{\partial r\left(u,v\right)}{\partial v} = 0 \tag{16}$$

3.7 The Mass Function

Generally speaking, it is very hard to give a precise definition of the amount of mass-energy contained within a closed surface, this is due to the gravitational waves that may transports energy through this surface, i.e. it defies a local description of such a quantity [10]. However, due to the absence of such issue in the spherically symmetric case, as we discussed before, we still can define this quantity as follows:
In Spherical symmetry, we can define *mass function* (or *Misner-Sharp mass* or *mass aspect function*) that describes a (generally speaking) quasi-local energy [13], as [18]:

$$m\left(t,r\right) = \frac{r}{2}\left(1 - g^{\mu\nu}\nabla_{\mu}r \cdot \nabla_{\nu}r\right) \tag{17}$$

we see that this function is constant on a particular sphere, thus it can be used to represent the active gravitational energy-mass inside it.
We note that in the limit $r \to \infty$, it approaches the *ADM mass* (equals to total mass-energy), thus this mass is just a special case of *Hawking mass* [10].
Also, noticing the condition of the apparent horizon criteria (16), we see that mass function

can be found immediately from $m = r_{Ah}/2$, where $r_{Ah}(u, v)$ is the zero of (16), i.e. the apparent horizon. However, using this relation in the simulation directly is not very accurate, as it will be explained latter.

4 Gravitational Collapse Process

Gravitational collapse happens when some system collapse due to it's internal forces that overcome any other "pushing away" forces.

4.1 Critical Phenomena in Gravitational Collapse

4.1.1 Introduction

Generally speaking, there are four kinds of the possible final states that a gravitational collapse can end in: a self-sustained object (such as stars), dispersion, black hole formation, and finally the formation of a naked singularity. However, in 1993, Choptuik [9] discovered during numerical simulations, that in the case of the spherical symmetry, the collapsing of matter with a massless scalar field as a source can end up only in one of two possible states: dispersion or black hole formation.
Moreover, he discovered that this system exhibits the behavior of the critical phenomena, which is characterized by the following properties:

- Critical Exponent (power law): There is a threshold p^* of some parameter p, where initial data depends on, such that, black holes formation starts from this threshold and below it the system disperse. Moreover, the mass of the created black hole scales as:

$$m \propto (p - p^*)^\gamma$$

  the case when $p < p^*$ is called *subcritical*, and leads to dispersion of scalar field to infinity, while $p > p^*$ called *supercritical*, and leads to black hole formation.
  (as a side note, this relation can be also obtained from perturbation analysis of scale-invariant variables of the problem).

- Universality: the critical exponent γ is a universal parameter relative to the initial data. That is, it is independent of the used family of one parameter' initial data. However, it still depends on the type of collapsing matter, and also if the cosmological constant is considered or not.

- Self-Similarity (or scale invariance): just before black hole formation, in the regions where the curvature is very large, space-time approaches a self-similar solution, that

is also universal in respect to the initial data. This solution is called *critical solution* ($p = p^*$), it also implies scale-invariance of the critical exponent. That is, the critical solution exhibits the following scale invariance independence of the initial data:

$$G^* (r, t) = G^* \left(e^{\Delta} r,\, e^{\Delta} t\right)$$

for some Δ (called, *echoing period/parameter*).

Speaking of the dynamical systems, in phase space, the critical solution is an attracting point on the critical surface that divides the space into two regions, one leads to dispersion, another one to the black hole formation (see figure 5)

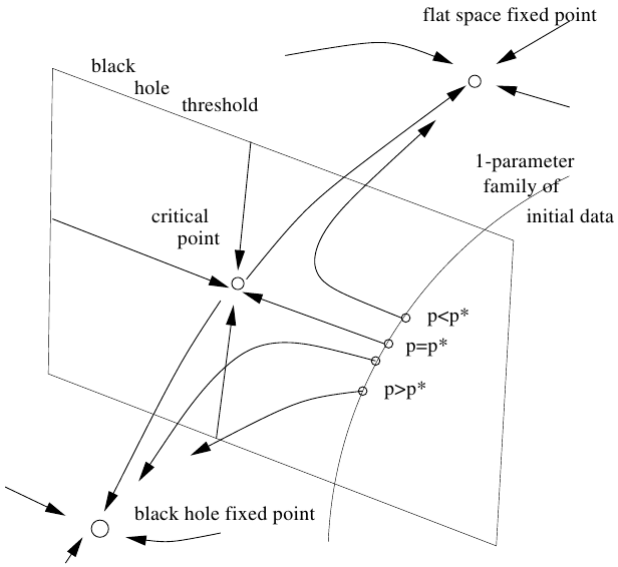

Figure 5: A phase space picture, that describes the critical phenomena.[9]

Later on, this behavior was reproduced in other cases, like in axial symmetry, charged black holes, and black holes with angular momentum, and this supports Choptuik's conjecture about the universality of this phenomena

The existence of the critical behavior is explained as a direct result of a dynamical competition: roughly speaking, the kinetic energy of the massless field tends to disperse itself to infinity, while the gravitational potential energy, if sufficiently dominant during the collapse will eventually result in trapping some amount of the mass-energy, inside the black hole [9]. It is worth noting that, the existence of the critical solution, means that some regions of the arbitrarily large curvature can be also achieved outside of the black hole, hence naked singularities may appear, in a contradiction to the *cosmic censorship conjecture* due to Penrose. However, this question is still open, because Christodoulou showed that naked singularity formation is not generic.

4.1.2 Types of Critical Phenomena

It was recognized later on, that there are two types of critical phenomena:

- Type I: in this case, the critical solution is stationary, or time-periodic (in contrast to self-similarity as in Type II). Also, the formed black hole will have a finite mass (see figure **??**) and can be thought of as a metastable star. The universality property, in this case, means that black hole mass near the threshold, is independent of initial data. Also in critical exponent law, the main role will be played not by the black hole mass, but by the lifetime of the intermediate state t_p, and it can be approximated by the critical solution as follows:

$$e^{t_p} \propto \frac{1}{(p-p^*)^\gamma}$$

- Type II: in this case, black hole mass can take any value, and a fixed critical point exhibits self-similarity symmetry, i.e. scale-invariant. These symmetries can be one of two types:

  - Continuous self-similarity : this happens, for example, when the matter behaves like a perfect fluid. In coordinates (τ, x^a), with a time-killing vector field, this means the following relation of metric coefficients:

$$g_{\mu\nu}(\tau, x^a) = e^{-2\tau}\tilde{g}_{\mu\nu}(x^a)$$

  - Discrete self-similarity: can be found in spherical, as well as axial symmetry, in this case, metric coefficients related as:

$$g_{\mu\nu}(\tau, x^a) = e^{-2\tau}\tilde{g}_{\mu\nu}(\tau, x^a) \ : \ g_{\mu\nu}(\tau+\Delta, x^a) = g_{\mu\nu}(\tau, x^a)$$

    where Δ is the echoing period. It should be noted, that in this case, the critical exponent actually has a small wiggle (that is, it has additional periodic terms [17]), as been discovered after Choptuik.

Many systems, like in the case of massive scalar field [7], exhibit both type I and II critical phenomena, depending on some special criteria. More precisely, for the mentioned example, type-II is observed only when the *Compton wavelength* $1/m$ of the scalar massive field, is much larger than the radial width, of the scalar field pulse, that induced the collapse. Otherwise, the type-I phase transition takes place.

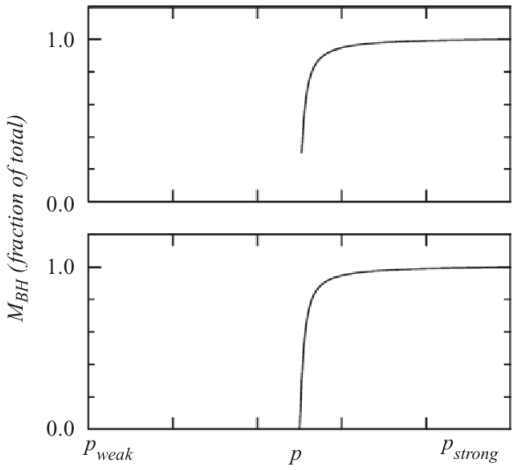

Figure 6: Schematic illustration of the possible black-hole threshold behavior. For a Type I (Top) transition, where the "order parameter", which is black hole mass, is nonzero near the threshold. While Type II (bottom) transition, takes place when the mass is infinitesimal at the critical point [9].

These types of critical phenomena are named after the first and the second-order phase transition in statistical mechanics:

- If we consider the liquid-gas phase transition, fluid density changes discontinuously. However, increasing the temperature up to the critical point T^*, makes the difference between gas and liquid density (which is the order parameter in this case) becomes indistinguishable. Actually, it changes as $\rho_{liq} - \rho_{gas} \propto (T^* - T)^\gamma$. This happens because the fluctuations become too large, that they even outsize the atomic scales. This indicates that the fluid near the critical point is approximately scale-invariant. This is a Type-II transition.

- While in the case of the ferromagnetic, they exhibit spontaneous magnetization, in low-temperature environments (even with the absence of an external magnetic field). It is spontaneous due to rotational symmetry: magnetization takes a random choice of direction, however, by increasing the temperature, the magnetization $\vec{m}$ decreases (this is the order parameter), till it finally vanishes at the Curie temperature T^*: $\|\vec{m}\| \propto (T^* - T)^\gamma$. However, the difference from the Type-II transition arises when we have also some weak external magnetic field $\vec{B}$. Obviously, it will break the above-mentioned rotational symmetry. But, up to the first order of accuracy, magnetization strength is independent of this external field, thus, having $\vec{m}(\vec{B}, T)$, we see that magnetization will change discontinuously at $\vec{B} = 0$. This is a Type-I transition, and for example, the initial angular momentum of the black hole can be represented as $\vec{B}$, while the final one, as $\vec{m}$.

4.2 Massless Scalar Field

The massless scalar field plays the role of a gravity source in the current problem, so here we mention some of the equations that are related to this setup.

For a massless scalar field, *Klein-Gordon equation* reduces to a simple wave equation:

$$\Box_g \varphi = \partial_\nu \left(\sqrt{-g}\, g^{\mu\nu} \partial_\mu \varphi \right) = 0$$

where $\Box_g$ is *D'Alember operator* with respect to the metric.
In spherical symmetry, this reduces to:

$$r\varphi_{,uv} + r_{,u}\varphi_{,v} + r_{,v}\varphi_{,u} = 0 \tag{18}$$

And the energy-impulse tensor of this scalar field is:

$$\mathcal{T}_{\mu\nu} = \varphi_{,\mu}\varphi_{,\nu} - \frac{1}{2} g_{\mu\nu} g^{\alpha\beta} \varphi_{,\alpha}\varphi_{,\beta}$$

4.3 Equations Setup

Due to the structure of the massless scalar field energy-impulse tensor, it's more convenient to use the trace form of Einstein equations:

$$\begin{aligned} \mathcal{R}_{\mu\nu} - \Lambda g_{\mu\nu} &= 8\pi \left(\mathcal{T}_{\mu\nu} - \frac{1}{2} g_{\mu\nu} \mathcal{T} \right) \\ \Rightarrow \mathcal{R}_{\mu\nu} &= 8\pi \varphi_{,\mu}\varphi_{,\nu} \end{aligned} \tag{19}$$

and by using the metric (13), this gives us the following equations:

$$4\pi r \varphi_{,u}^2 - 2\frac{\alpha_{,u}}{\alpha} r_{,u} + r_{,uu} = 0 \tag{20a}$$

$$4\pi r \varphi_{,v}^2 - 2\frac{\alpha_{,u}}{\alpha} r_{,v} + r_{,vv} = 0 \tag{20b}$$

$$4\pi \varphi_{,u}\varphi_{,v} - \frac{\alpha_{,u}\alpha_{,v}}{\alpha^2} + \frac{\alpha_{,uv}}{\alpha} + \frac{r_{,uv}}{r} = 0 \tag{20c}$$

$$r r_{,uv} + r_{,u} r_{,v} + \frac{\alpha^2}{4} = 0 \tag{20d}$$

(they corresponds to the $uu, vv, \theta\theta, uv$ components of Einstein equations, correspondingly).

5 Numerical Methods

During the past years, big developments and many suggestions were introduced to make the numeric methods, that are related to the current problem, more accurate and efficient,

but also more complex. In this work, we have chosen to use the simplest possible approach, that can also achieve reasonable results (comparing to previous works) in replicating critical phenomena behavior.

5.1 Preparing Einstein Equations

In numerical analysis, we need to reduce the equations (20a) to the first-order differential equations. For this, we introduce the following set of auxiliary variables (the same variables are used in the source code, note that we are using two-letter variable names):

$$
\begin{aligned}
Au &\equiv \frac{\alpha_{,u}}{\alpha} \quad , \qquad Av \equiv \frac{\alpha_{,v}}{\alpha} \\
Ru &\equiv r_{,u} \quad , \qquad Rv \equiv r_{,v} \\
\Phi &\equiv \sqrt{4\pi G}\varphi \\
Fu &\equiv \Phi_{,u} \quad , \qquad Fv \equiv \Phi_{,v}
\end{aligned}
$$

then, all of the needed equations are mentioned in the following table 1.

Label	Equation	Class	Source
E01	$\alpha_{,u} = \alpha \cdot Au$	Ignored	Auxiliary Variables
E02	$\alpha_{,v} = \alpha \cdot Av$	Constraint	
E03	$r_{,u} = Ru$	Ignored	
E04	$r_{,v} = Rv$	Constraint	
E05	$\Phi_{,u} = Fu$	Ignored	
E06	$\Phi_{,v} = Fv$	Constraint	
E07	$Fu_{,v} = -\frac{1}{r}\left(Ru \cdot Fv + Rv \cdot Fu\right)$	Constraint	(18)
E08	$Fv_{,u} = -\frac{1}{r}\left(Ru \cdot Fv + Rv \cdot Fu\right)$	Evolution	
E09	$Au_{,v} = \frac{1}{r^2}\left(Ru \cdot Rv + \frac{\alpha^2}{4}\right) - Fu \cdot Fv$	Ignored	(20c) + E11,12
E10	$Av_{,u} = \frac{1}{r^2}\left(Ru \cdot Rv + \frac{\alpha^2}{4}\right) - Fu \cdot Fv$	Evolution	
E11	$Ru_{,v} = -\frac{1}{r}\left(Ru \cdot Rv + \frac{\alpha^2}{4}\right)$	Constraint	(20d)
E12	$Rv_{,u} = -\frac{1}{r}\left(Ru \cdot Rv + \frac{\alpha^2}{4}\right)$	Control	
E13	$Ru_{,u} = 2Au \cdot Ru - r \cdot Fu^2$	Ignored	(20a)+(20b)
E14	$Rv_{,v} = 2Av \cdot Rv - r \cdot Fv^2$	Constraint	

Table 1: List of all first order equations that represents evolution, constraints and auxiliary equation that will be used in simulation. All of them, are written in the form $dY/dx = F\left(Y, x\right)$, which is the suitable form for the numeric methods that we will use. Also, all of them can be obtained easily by simple substitution of the auxiliary variables in the corresponding equations that mentioned in the "source" column.

This set of the equations are not really independent, hence, some of them can be ruled out:

- First of all, noticing the expressions for Mass function (17) and Ricci scalar (19), we note that there is no need to calculate the auxiliary variable Au, this immediately drops (as mentioned in the "Class" column of the table 1) each of the equations: E01, E09, and E13 [2]. While E01, E03, and E05 are not used in evolution directly, although, they will be used in the boundary conditions (as we will see later on), or the correspondent variables will be found explicitly latter by PECECE method.

- We notice that the auxiliary variables Av, Fv, have solely evolution equations (since there is no $Av_{,v}, Fv_{,v}$). And in contrast to that, the auxiliary variables Au, Fu have no evolution equations at all, hence, this can be understood as a characteristic of the Cauchy problem in general relativity. So. each of the E8, E10 equations, should be considered evolution equations.

- The equation E12 is not needed basically, anyway we will use it to control the errors, and for the stability of the numerical methods.
- The remaining equations are just constraints on the initial Cauchy surface, which can be considered as a null surface with $u = const \equiv 0$.

By this, we end up with 6 constraint equations, and 2 evolution equations.

5.2 Boundary Conditions

Regularization of spherically symmetric evolution in numeric methods, and setting up the Cauchy problem, is not a trivial problem, for example see [14] for a detailed treatment.
For this, on-axis, we impose a *local flatness condition* [14], which means that at the origin, we assume that we have a flat metric, that is:

$$\lim_{r\to 0} g_{\mu\nu} = \eta_{\mu\nu}$$

From this, we get the following two boundary conditions:

1. The metric element:
$$d\ell^2 \equiv \alpha^2(u,v)\, du dv - r^2 d\Omega^2$$
has to become flat on-axis, that is:
$$d\ell^2 = dt^2 - dR^2 - R^2 d\Omega^2$$
so using (10) transformations, we see that it should be $dR = dr = \alpha d\rho^*$ on axis, or:
$$dr(u,v) = \alpha\frac{dv-du}{2} = \frac{\partial r}{\partial v}dv + \frac{\partial r}{\partial u}du$$
$$\Rightarrow \frac{\partial r}{\partial v} = -\frac{\partial r}{\partial u} = \frac{\alpha}{2} \Rightarrow Rv = -Ru = \frac{\alpha}{2}$$
(note that from E11, if $Ru = -Rv$, also implies $Rv = -Ru = \alpha/2$). Finally, E8 gives $Fv = Fu$ (all are on-axis).

2. Furthermore, a more detailed treatment [13] for flatness condition, leads to the following regularity boundary condition for α on-axis (we also require that our scalar field will be regular on-axis):
$$\left.\frac{\partial\alpha}{\partial r}\right|_{r=0} = \left.\frac{\partial\Phi}{\partial r}\right|_{r=0} = 0 \tag{21}$$
(note that this doesn't imply that they are constant in time at the origin, for example, $\alpha(u,u)$ is actually on-axis).

Because there is no need here to track the evolution of our system after black hole formation, we don't impose boundary conditions at null infinity, since we will stop simulation before anything is reflected from null infinity.

Now by using those boundary conditions, we can rewrite the proper time (15) on axis: we showed in the first boundary condition that $dr = \alpha d\rho^*$, and noticing that α is constant on-axis relative to areal coordinate, due to the second boundary condition, we can integrate previous relation at each fixed moment of time to get $r = \alpha\rho^* = \alpha\left(v-u\right)/2$, hence, $v\left(u,r\right) = 2r/\alpha + u$, and so $\partial_u v\left(u,r\right) = 2r\partial_u\alpha^{-1} + 1$. On-axis we have also $r = 0$, so $\partial_u v\left(u,r\right)|_{r=0} = 1$. All this leads to the following simple expression for the proper time on the axis $u = v$:

$$T\left(u\right)|_{r=0} = \int_0^u \alpha\left(\omega,\omega\right) d\omega \tag{22}$$

5.3 Initial Conditions

Here we note the following:

1. We have the freedom in choosing the initial scalar field. And by following the usual convection, we use Gaussian impulse on the null coordinate v:

   $$\varphi\left(0,v\right) \equiv Av^2 e^{-\frac{\left(v-v_0\right)^2}{\sigma^2}}$$

   Where the amplitude A, will play the role of the critical parameter in this work, and we have chosen such a form to fulfill regularity conditions that have been mentioned in the boundary conditions.

   However, for our problem, we are using $Fv\left(u,v\right)$ rather than the scalar field itself, thus we can easily find that:

   $$Fv\left(0,v\right) = 2A\cdot v\left[1 - \frac{v-v_0}{\sigma^2}v\right] e^{-\frac{\left(v-v_0\right)^2}{\sigma^2}}$$

2. In addition to that, we assume that initially we had a flat Minkowski space, so we put $\alpha\left(0,v\right) \equiv 1$ then $Av\left(0,v\right) = 0$, this condition actually equivalent to coordinate gauge fixing for v.

Finally, to avoid overflows when calculations just started, we will set the initial radial value, at the origin to some non-zero, but less than the grid step size, value. For example: $r\left(0,0\right) \equiv h/10$.

5.4 Finite Difference Method

Finite Differences (FD) approximates derivatives by combining nearby function values with some particular weights. Several different algorithms are available for calculating such weights. If $f_n \equiv f(x + n \cdot h)$ is some function, where h our uniform grid step, then by using Taylor series we can write that:

$$\frac{f_{n+1} - f_n}{h} - f' = \frac{h}{2!} f'' + \frac{h^2}{3!} f''' + O\left(h^3\right)$$

we are free to replace the grid step h, by its double value, to get the following:

$$\frac{f_{n+2} - f_n}{2h} - f' = 2\frac{h}{2!} f'' + 4\frac{h^2}{3!} f''' + O\left(h^3\right)$$

by multiplying the first equation by -2 and summing both equations, we can get rid of the first-order terms in h, and we find *second order accuracy forward difference* approximation of a derivative:

$$f' = \frac{-3f_n + 4f_{n+1} - f_{n+2}}{2h} + O\left(h^2\right)$$

we can use this result with the boundary condition (21), for example:

$$\left.\frac{\partial \alpha(t,r)}{\partial r}\right|_{r=0} = \frac{-3\alpha(t,0) + 4\alpha(t,h) - \alpha(t,2h)}{2h} + O\left(h^2\right)$$

on axis we have $u = v = t$, so we can relabel t by our null time-like coordinate u. Then, for example, in the last term we have $u = t - r \to u - 2h$ and $v = t + r \to u + 2h$, so:

$$\begin{aligned} \left.\frac{\partial \alpha(u,v)}{\partial r}\right|_{u=v} &\simeq \frac{-3\alpha(u,u) + 4\alpha(u-h,u+h) - \alpha(u-2h,u+2h)}{2h} = 0 \\ \Rightarrow \alpha(u,u) &\simeq \frac{1}{3}\left[4\alpha(u-h,u+h) - \alpha(u-2h,u+2h)\right] \end{aligned}$$

this will be our regularity condition on axis, similarly we have the same equation for φ, or in terms of auxiliary variables Φ .

We will need also to estimate derivatives in the control equation E12, and to avoid the errors in our "error estimation", we will use the more accurate 8^{th} *order accuracy centric finite-difference approximation* of derivatives (see appendix for derivation).:

$$f' = \frac{45\left(f_{n+1} - f_{n-1}\right) - 9\left(f_{n+2} - f_{n-2}\right) + \left(f_{n+3} - f_{n-3}\right)}{60h} + O\left(h^8\right)$$

5.5 Runge-Kutta methods

To solve E01-E14 differential equations, we will use 4^{th} order Runge-Kutta method, since it was done before successfully in many similar works (for example [3]).
Recalling the general equation form $dY/dx = F(Y, x)$ (the general form of table 1 equations), and for a step size h on the grid, the Rung-Kutta iteration method calls the next iteration Y according to the following formulas:

$$Y_{n+1} = Y_n + \frac{1}{6}\left[k_1 + k_4 + 2\left(k_2 + k_3\right)\right] \quad : \quad \begin{cases} k_1 & \equiv h\, f\left(Y_n, x\right) \\ k_2 & \equiv h\, f\left(Y_n + \frac{k_1}{2}, x_n + \frac{h}{2}\right) \\ k_3 & \equiv h\, f\left(Y_n + \frac{k_2}{2}, x_n + \frac{h}{2}\right) \\ k_4 & \equiv h\, f\left(Y_n + k_3, x_n + h\right) \end{cases}$$

But here we are facing the problem of evaluating the coefficients $k_{2,3}$, because we need to calculate the function f (and thus to calculate different auxiliary variables) at locations that are in "between" of the grid points. To resolve this, we may naively consider using the average of the function's value, in the nearest two grid points:

$$f\left(Y, x + \frac{h}{2}\right) \simeq \frac{1}{2}\left[f\left(Y, x\right) + f\left(Y, x + h\right)\right]$$

However, due to the non-linearity, and high volatility of the solution, near the critical parameter, or during Black hole formation, applying this method directly to evolution parameters will result in unstable calculations. To resolve this, different methods are suggested (such as mesh refinement, multi-domain decomposition, and pseudo-spectral collocation). Here we are going to use maybe the simplest possible method, that had been suggested in [3].

5.6 Explicit PECECE Method and Stiffness

This method is an algorithm that proceeds in two steps. The first one, a prediction step, calculates a rough approximation of the desired quantity. The second one, a corrector step, refines the initial approximation by using a specially constructed average.
The basic *Predict–Evaluate–Correct–Evaluate* (PECE) algorithm (or *Heun's method*), is based on the *Euler method* (which is an explicit method), jointly with the *trapezoidal rule* (an implicit method).
If we have the differential equation $y' = f(t, y)$, then:

1. Predictor step: calculates a rough approximation of the desired quantity. Starting from

the current value y_i, calculate an initial guess value for $\tilde{y}_{i+1}$, via the Euler method:

$$\tilde{y}_{i+1} = y_i + h\, f\left(t_i, y_i\right)$$

2. Corrector step: refines the initial approximation using another average. We improve the initial guess using the trapezoidal rule,

$$y_{i+1} = y_i + \frac{1}{2} h \left[f\left(t_i, y_i\right) + f\left(t_{i+1}, \tilde{y}_{i+1}\right)\right]$$

which is the value that we will use for the next iteration step.
This last corrector step can be actually applied multiple times (so we get our PECECE for example, as explained below), leading hopefully to a more accurate and stable result.

In order to avoid also stiffness (it is a phenomena when one needs to use an extremely small step in the numerical methods, to maintain method's stability, even when the solution is smooth), in Runge-Kutta methods with the nonlinear equations as in general relativity, PECE can be used.
The basic idea behind PECE, is to replace $\tilde{y}_{i+1}$ in the corrector step equation, with y_{i+1}, and we assume that the function f, is simple enough to solve the resultant equation explicitly relative to y_{i+1}, then by applying the corrector step again, on the resultant y_{i+1}, it will give us more stable results.

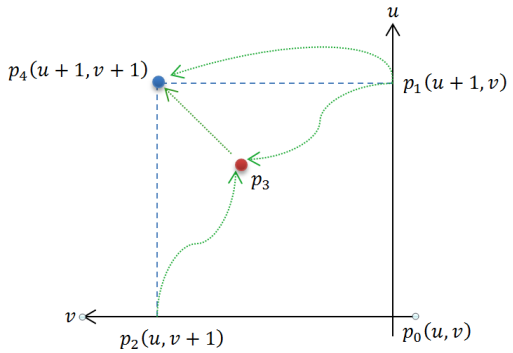

Figure 7: A scheme of PECECE calculations pipeline.

In our problem, the predictor step will be the evolution of our parameters, while the corrector step will be used to calculate the intermediate values in constraint equations, and by solving it explicitly, we can get the corrected values for the evolution parameters, as follows (see figure 7):
Let $e_{,u} \equiv F\left(c, e\right)$ will represent any of the evolution equation E08,E10, where e represent the evolution parameters, and c represents some constraint parameter. Similarly, let $c_{,v} \equiv G\left(c, e\right)$

represent any of the other constraint equations, then we have:

$$\begin{cases} e\left(p_3\right) = e\left(p_1\right) + hF\left(c\left(p_1\right), e\left(p_1\right)\right) \\ c\left(p_3\right) = c\left(p_2\right) + \dfrac{h}{2}\left[G\left(c\left(p_2\right), e\left(p_2\right)\right) + G\left(c\left(p_3\right), e\left(p_3\right)\right)\right] \end{cases}$$

by solving the last equation explicitly (see the below solved variants) relative to $c\left(p_3\right)$, and then applying the corrector step again on the evolution equation, we get:

$$\begin{aligned} e\left(p_4\right) &= e\left(p_1\right) + \frac{h}{2}\left[F\left(c\left(p_1\right), e\left(p_1\right)\right) + F\left(c\left(p_3\right), e\left(p_3\right)\right)\right] \\ &= \frac{1}{2}\left[e\left(p_3\right) + e\left(p_1\right) + hF\left(c\left(p_3\right), e\left(p_3\right)\right)\right] \end{aligned}$$

The direct solutions according to the above scheme, for the needed evaluation variables, are presented in table 2.

Label	Equation	Source
M1	$\alpha_3 = \alpha_2 \cdot \dfrac{2 + h \cdot Av_2}{2 - h \cdot Av_3}$	E02
M2	$r_3 = r_2 + \dfrac{h}{2}\left[Rv_2 + Rv_3\right]$	E04
M3	$Rv_3 = \dfrac{Rv_2 + \dfrac{h}{2}\left(2Av_2 \cdot Rv_2 - r_2 \cdot Fv_2^2 - r_3 \cdot Fv_3^2\right)}{1 - h \cdot Av_3}$	E14
M4	$Ru_3 = B\left[Ru_2 - \dfrac{h}{2}\left(\dfrac{Ru_2 \cdot Rv_2 + \alpha_2^2/4}{r_2} + \dfrac{\alpha_3^2/4}{r_3}\right)\right]$	E11
M5	$Fu_3 = B\left[Fu_2 - \dfrac{h}{2}\left(\dfrac{Rv_2 \cdot Fu_2 + Ru_2 \cdot Rv_2}{r_2} + \dfrac{Ru_3 \cdot Rv_3}{r_3}\right)\right]$	E07

Table 2: A list of the explicit solutions for the corresponding equations. For brevity, we replaced the evaluation point, with its index, for example $r_3 \equiv r\left(p_3\right)$, and $B \equiv 1/\left(1 + \frac{h}{2}\frac{Rv_3}{r_3}\right)$.

Note that besides evolution variables, we also found the evolving equations for the corresponding constraint variables, since we need them as an intermediate parameters/steps, to calculate evolution variables.

5.7 The Algorithm

Now we can line out a scheme of the used algorithm to perform our calculations:

1. Set the initial value of the scalar field on-axis and another auxiliary variables at the origin, as mentioned before.

2. At the initial moment of time, because no evolution is started yet, we:

(a) Set the boundary conditions on-axis and at the origin.

(b) Cycle through each v, and integrate all constraint auxiliary variables (by using Runge-Kutta).

3. Start cycling along with all slices of u (except the first one, since it has been handled above), and within each slice we:

   (a) Set the boundary conditions on-axis (by using finite difference equations) for the current slice' variables.

   (b) "Initial" values of the evolution variables on-axis are inherited/copied from the previous slice.

   (c) Cycle through each v and:

      i. Evolve our two evolution variables up to the current slice (and other intermediate constraint variables, as explained in the explicit PECECE method).

      ii. Integrate all constraint auxiliary variables (by using Runge-Kutta) in the current slice.

4. Do the rest of the things, like calculating proper time, printing out the results, etc...

6 Simulation Results

6.1 Some Technical Notes

- To find the event horizon, we used the obtained condition (16). So we check each slice for Rv sign change. However, due to possible numerical artifacts, it is possible that there will be a couple of zeros for this quantity. In fact, It can be shown [15] that there can be only one null for Rv along a single slice. But since we don't know for sure which zero is the real one, we are going along with the given slice, to find the zero that corresponds to the maximum value for areal coordinate r.

- To find the critical parameter, we perform multiple simulations starting from some range, then by halving it, we check on which half of the range collapse took place, then we choose to repeat the operation again and again, till we arrive at the needed accuracy. Note that, technically speaking, for the particular initial parameters, and grid size, one can achieve pretty high accuracy (limited by rounding errors). However, this is only apparently accurate, as we would explain below.

- Because our grid size is limited (to the computer memory resources), we can't decrease the step size to arbitrarily small values, this may lead us also to lose the apparent horizon formation (it could form outside of the grid). For example, by using the case mentioned

in table 3, a critical apparent horizon will form approximately at $v_h = 0.138$ (it's hard to find it exactly due to the reasons explained below). So, for a grid of 5000×5000 points, we are forced to use a step length not less than $h \simeq 0.15/5000 = 0.00003$ (we used a bigger v_h here, due to the left/right region squeezing as mentioned above). We can use this fact to tune the initial parameters of the scalar field, such that we force the horizon formation to be very close to the origin, and hence we can decrease step size to a reasonable value (to get a more accurate critical parameter estimation), while still controlling the horizon formation process to stay within the grid.

- There is a great uncertainty in finding the accurate value for the critical parameter (at least in the scope of this algorithm). This can be easily seen by decreasing the step size. Roughly speaking, we found that step size affects accuracy of critical parameter extremely slowly. For example (see table 3) decreasing the step 100 times, allows us to calculate critical parameter only $13 - 18$ times better, this makes calculations/plots that are related to the critical parameter value, very vage. However, for a fixed step size, small errors in the calculated critical value, will still produce the expected collapse/dispersion behavior for the scalar field.

h	0.003	0.0009	0.0001	0.00005	0.00003
A^*	7.61730	7.61910	7.61176	7.61240	7.61267

Table 3: This table shows how slowly is the accuracy of critical amplitude increases, when we decrease step size. Those values are calculated for the following initial parameters for the scalar field $(v_0, \sigma) = (0.1, 0.01)$.

- For the graphics in the following paragraph, we will use the initial values $(v_0, \sigma) = \left(2, 1/\sqrt{2}\right)$ on a grid 4000×4000, with a step size equals to 0.0025 (since for the minimally possible step size of 0.0009, the critical apparent horizon will form approximately at $v_h = 4.4982$, and the critical parameter is about 0.051348). Those values are chosen because they gives us visually more expressive graphics, and because they are close to the one used in [3].

- As a simple validation for numerical methods, one tries to see if the algorithm will produce a flat Minkowski space when there is no source or scalar field. However, this is still a very rough way for algorithm validity testing.

6.2 Comparing Sub- and Super-Critical Cases

First of all, it is interesting to see how the areal coordinate and its derivative differs in both cases (i.e sub- and super-critical). This will also show clearly, that the black hole is formed

due to (16). The results are presented in the below the table:

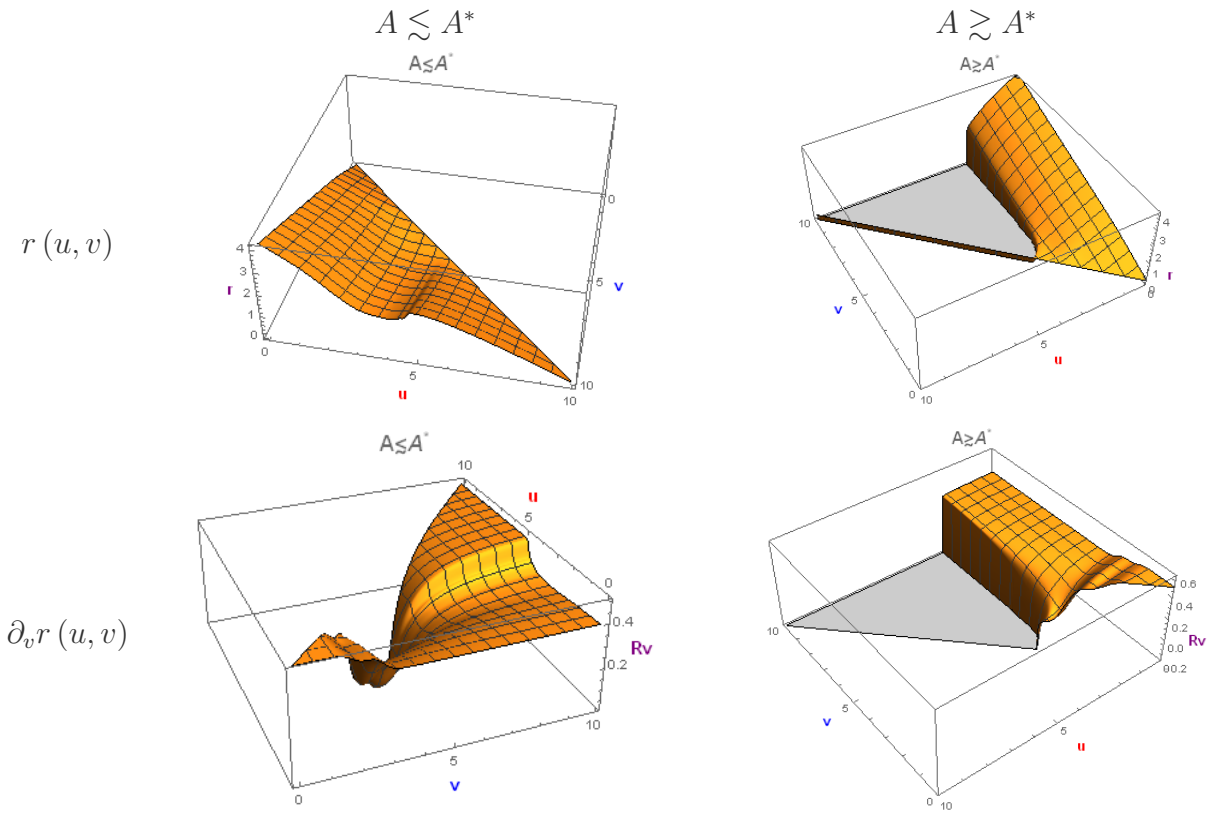

Figure 8: Comparing how the areal coordinate evolves in a slightly super-, and slightly sub-critical cases. Grayed areas shows where our numerical methods breaks down.

However, viewing it in $3D$ maybe not most obvious approach, so below we provide a view of different nearby slices :

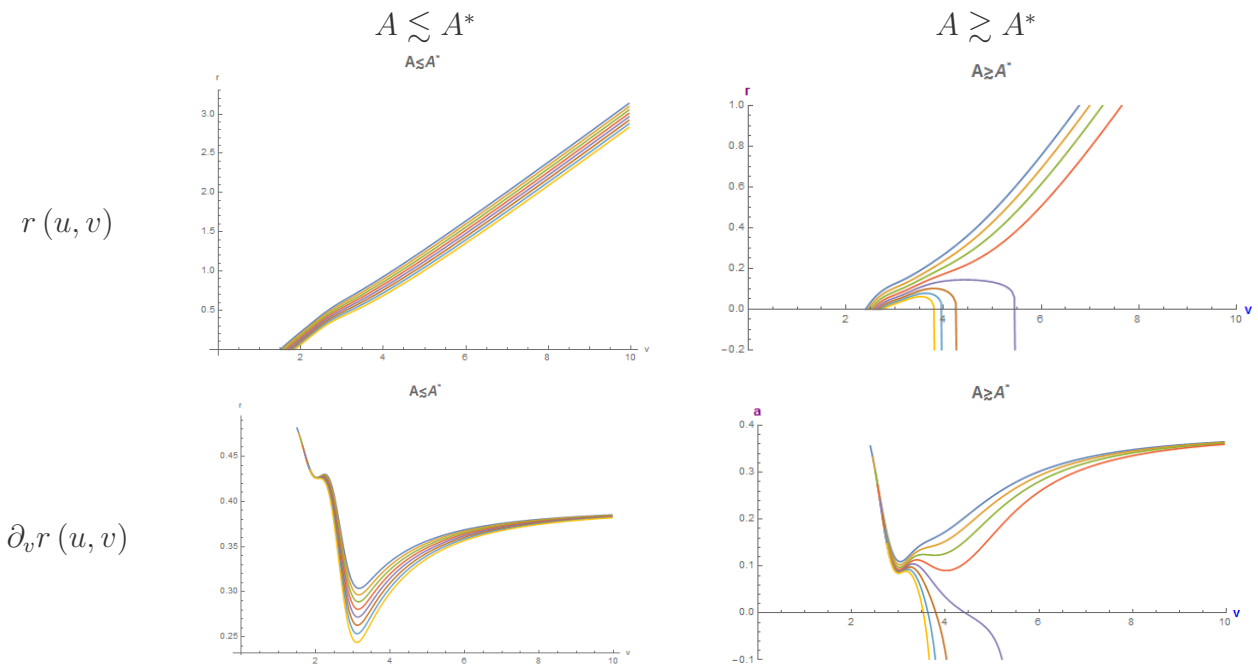

Figure 9: A bunch of slices from the previous $3D$ graphics, so that it will be clear how the behavior of the areal coordinate radically changes between the both cases. Whenever our code is broken down, we set $y-$ axis value to -1.

Here it's clear how the derivative $\partial_v r$ starting from some slice (time) changes its sign at $v_h \simeq 4.5$, and signaled by the apparent horizon formation. Hence, this point corresponds to the maximum value of r, according to which, we can calculate black hole mass by (17). Also, we note that once the black hole is formed, the areal coordinate becomes zero, forming by that the farthest possible closed trapped region. Also, it should be clear now what was meant by the non-penetrating coordinates. This results are consistent with previous works like [3] and [16].

Furthermore, our point of interest is how the scalar field behaves and evolves, simulation gives us:

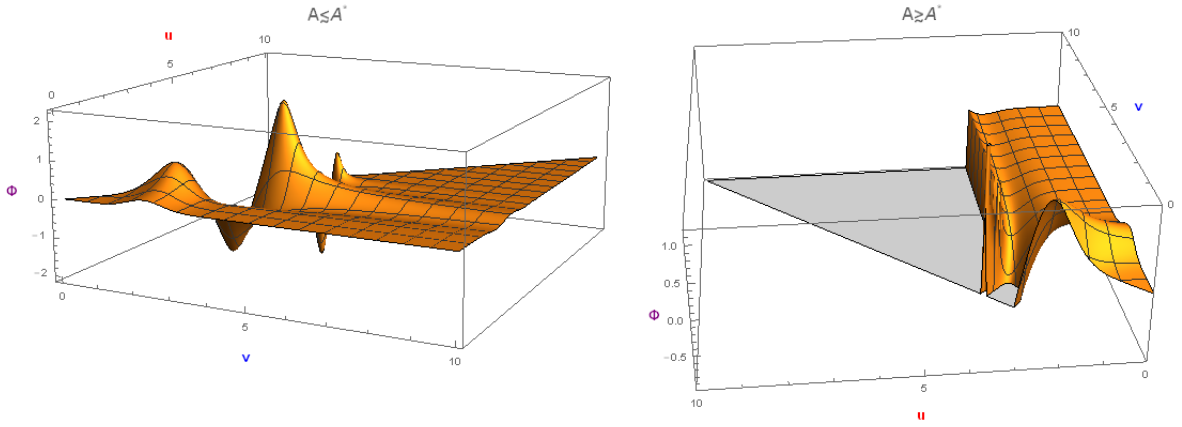

Figure 10: Comparing how the scalar field Φ is evolving in both cases.

While we can see how the scalar field starts with a small Gaussian impulse, it oscillates on-axis and then disappears in space in the sub-critical case, while in the super-critical case, the oscillation starts but once a black hole is formed, those oscillations will be immediately trapped behind the apparent horizon, exactly as the *no-hair theorem* predicts. Furthermore, the sub-critical plot was made very close to the critical case, to show clearly at least some oscillations, this hints us at the self-similarity behavior, that will be presented in the next paragraph, in a much clearer way.

Also, now we would like to compare how α behaves in both cases:

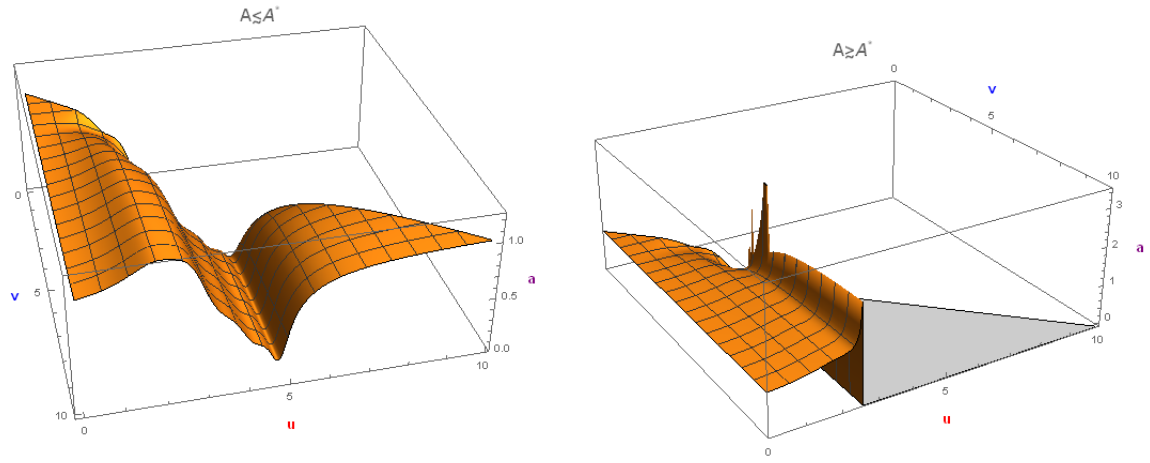

Figure 11: Comparing how the conformal factor α is evolving in both cases.

For the sub-critical case, we see that even so, α evolves with scalar field, it will eventually approach 1, that is, a flat space. But in the super-critical case, it stays very close to 1, till black hole formation process starts, then it begins to increase very rapidly, until our numerical methods get broken down.

6.3 The Critical Behavior

First of all, we would like to see how the self-similarity shows up in the critical state. For that, we examine how the scalar field behaves on-axis at very close values to the critical parameter (from left and right):

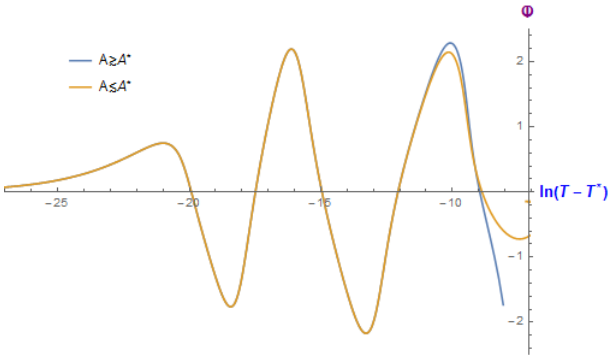

Figure 12: A plot that shows the self-similarity behavior of the scalar field, on-axis, near-critical state.

We see from this plot, that the behavior of the scalar field, near the critical parameter, exhibits self-similarity as described by Chupkin. Also, the fact that it follows this behavior either in a slightly sub-critical or super-critical case, confirms the universality property.
From this plot, we can estimate the echoing parameter, which is $\Delta \simeq 16.12 - 10.13 \simeq 6$. This is about twice bigger than the value reported by various other authors ($\Delta \simeq 3.44$ by [12] and [2]). It is known that determining T^* can't be accurate in general, also it could be due to using a $10-$based logarithms, instead of using the natural logarithm, as can be found in

some reports.
We can now check how the Ricci scalar exhibits self similarity near critical state:

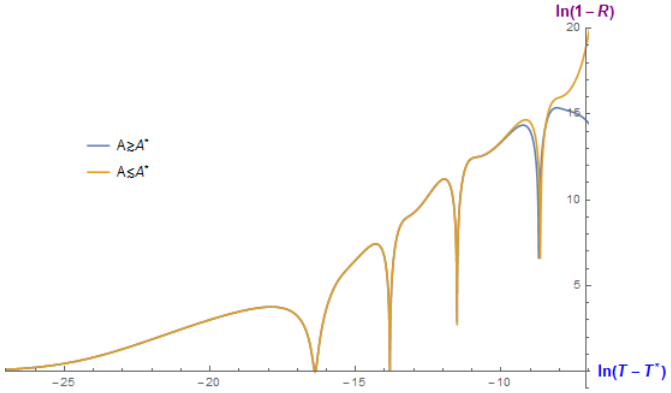

Figure 13: A plot that shows the self-similarity behavior of Ricci scalar on axis, near critical state.

As we see, it is also an oscillation, and actually it grows as $e^{2\Delta}$, from which we calculate $2\Delta \simeq 3.65$, and that the oscillations happens with a period of 2.6 in average.
Finally, we need to find the critical exponent:

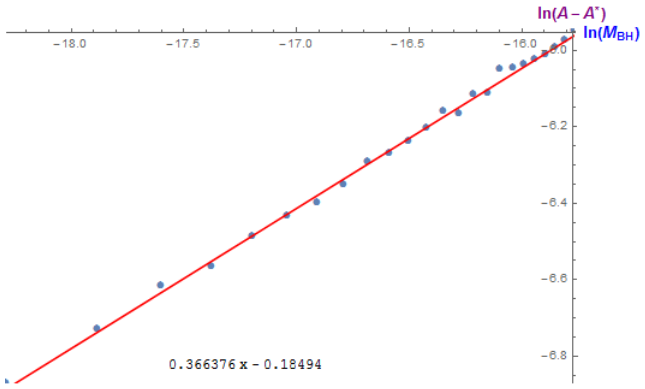

Figure 14: A plot that shows the critical exponent that related to the black hole mass.

We see that the slope of the linear fit is about $\gamma \backsimeq 3.37$, which is very close to the value of 3.36 in [12] and 3.374 in [14]. However, we found that at different regions of the distances from the critical parameter $A - A^*$, we may get different slope values (that is, in general, we don't have a strictly linear relation as it should be, but a smooth curve instead). So we have chosen the range that gives the closest values to the previously reported values. Of course, the uncertainty in determining accurately the critical parameter also plays an important role in this discrepancy. However, it seems that similar behavior was also observed in [15]. We may also consider the above region to be the best region of amplitudes, where our numerical methods work correctly.

6.4 Accuracy of The Calculations

Finally, it's interesting to examine the accuracy of our calculations, thus we plot how the control equation E12, and how it diverges from zero:

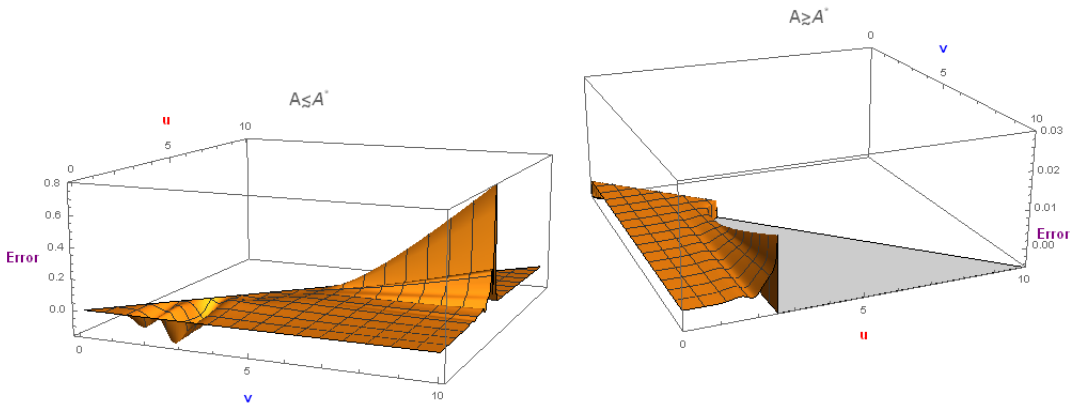

Figure 15: Comparing calculation error by equation E12 in both cases.

we see from those plots, that generally speaking, the error stays within a reasonable range to reproduce critical phenomena. Because the sub-critical case is very close to the critical one, we can observe at some points a big spike of errors, this happens because the black hole tries to form but fails. This also explains why detecting the accurate value for the critical parameter is quite tricky. On another hand, for the super-critical case, the error stays very reasonable till the black hole formation, then the error increases in a very fast manner till our methods break down.

7 Appendixes

7.1 Deriving 8^{th} Order Accuracy Centric Finite Difference Approximation

By using the Taylor series, we can write the *forward and backward difference* (relative to h) as:

$$\frac{f_{n+1}-f_n}{h}-f'=\frac{h}{2!}f''+\frac{h^2}{3!}f'''+O\left(h^3\right)$$

$$\frac{f_n-f_{n-1}}{h}-f'=-\frac{h}{2!}f''+\frac{h^2}{3!}f'''+O\left(h^3\right)$$

by summing them up, we can get rid of all odd order terms in h, and we will get the *centered difference*:

$$\frac{f_{n+1}-f_{n-1}}{2h}-f'=\frac{h^2}{3!}f'''+\frac{h^4}{5!}f^{(5)}+O\left(h^6\right) \tag{23}$$

we can replace in the last equation, the step h by $2h$, or even $3h$, to get:

$$\frac{f_{n+2}-f_{n-2}}{4h}-f'=4\frac{h^2}{3!}f'''+16\frac{h^4}{5!}f^{(5)}+O\left(h^6\right)$$

$$\frac{f_{n+3}-f_{n-3}}{6h}-f'=9\frac{h^2}{3!}f'''+81\frac{h^4}{5!}f^{(5)}+O\left(h^6\right)$$

if we subtract from those equations (23) (multiplied by a suitable constant), we can get rid of second-order terms in h:

$$\frac{8\left(f_{n+1}-f_{n-1}\right)-\left(f_{n+2}-f_{n-2}\right)}{12h}-f'=-4\frac{h^4}{5!}f^{(5)}-20\frac{h^6}{7!}f^{(7)}+O\left(h^8\right)$$

$$\frac{27\left(f_{n+1}-f_{n-1}\right)-\left(f_{n+3}-f_{n-3}\right)}{48h}-f'=-9\frac{h^4}{5!}f^{(5)}-90\frac{h^6}{7!}f^{(7)}+O\left(h^8\right)$$

there is no reason to favor one of these equations, that are evaluated at $f_{i\pm3}$ or $f_{i\pm2}$, over another. But we can get rid of the 4^{th} and 6^{th} order terms in h, by mutilating by a suitable number, and subtracting those equations, to get the final result:

$$f'=\frac{45\left(f_{n+1}-f_{n-1}\right)-9\left(f_{n+2}-f_{n-2}\right)+\left(f_{n+3}-f_{n-3}\right)}{60h}+O\left(h^8\right)$$

References

1. Luciano Rezzolla, “An Introduction to Gravitational Collapse to Black Holes”, SISSA, International School for Advanced Studies and INFN, Trieste, Italy 2004

2. R. S. Hamade and J. M. Stewart, Class.Quant.Grav. 13, 497 (1996), gr-qc/9506044

3. Miguel Francisco Garcıa Vera , “Gravitational collapse in asymptotically flat and asymptotically anti-de-sitter spacetime”, 2012

4. Thomas W. Baumgarte, Stuart L. Shapiro, “Numerical Relativity: Solving Einstein’s Equations on the Computer” , ISBN-13 978-0-511-72937-9 , 2010

5. Hawking, S. W. and G. F. R. Ellis (1973). “The large scale structure of space-time”. Cambridge University Press, Cambridge.

6. Sean A. Hayward, “Black-hole dynamics in spherical symmetry”, 2013

7. Brady, P.R., Chambers, C.M. and Gonc¸alves, S.M.C.V., “Phases of massive scalar field collapse”, Phys. Rev. D, 56, R6057–R6061, (1997), DOI:10.1103/PhysRevD.56.R6057, arXiv:gr-qc/9709014.

8. Éric Gourgoulhon , “3+1 Formalism in General Relativity: Bases of Numerical Relativity”, Springer, ISBN 978-3-642-24524-4, 2012

9. Choptuik, M. (1998). “The (Unstable) Threshold of Black Hole Formation”. In N. Dadhich and J. Narlikar (Eds.), Gravitation and Relativity: At the Turn of the Millennium, pp. 67–86. Inter-University Centre for Astronomy and Astrophysics, Ganeshkhind, Pune.

10. Ingemar Bengtsson, “Spherical symmetry and black holes”, 2012.

11. Kramer D., “Axially symmetric stationary solutions of the projective field theory”. (in german) , Acta Phys.Polon. B2 (1971) 807-811

12. M. W. Choptuik, “Universality and scaling in gravitational collapse of a massless scalar”, Phys. Rev. Lett. 70, 9 (1993).

13. Michael Purrer , “Global versus Local Aspects of Critical Collapse”, gr-q/0708.1914, 2007

14. Miguel Alcubierre and Jose A. Gonzalez, “Regularization of spherically symmetric evolution codes in numerical relativity”, gr-qc/0401113, 2004

15. Roland Stevenson, “The Spherically Symmetric Collapse of Collisionless: Matter Exploring Critical Phenomena through Finite Volume Methods”, 2005

16. Tomohiro Harada and B. J. Carr, “Growth of primordial black holes in a universe containing a massless scalar field”, Phys. Rev. D, 2005, DOI: 10.1103/PhysRevD.71.104010

17. Carsten Gundlach and Jose M. Martın-Garcıa, “Critical Phenomena in Gravitational Collapse”, Living Rev. Relativity, 10, (2007), 5 , 2010

18. Гладуш В.Д., “Геометрические Методы в Теории Релятивистских Конфигураций”, удк 530.12; 531.51